Composite Structures 300 (2022) 116151

Contents lists available at ScienceDirect

Composite Structures

journal homepage: www.elsevier.com/locate/compstruct

Tailored twist morphing achieved using graded bend–twist metamaterials

Huaiyuan Gu [a,*], Javad Taghipour [b], Alexander D. Shaw [b], Mohammadreza Amoozgar [c], Jiaying Zhang [d,f], Chen Wang [e], Michael I. Friswell [b]

[a] Department of Aerospace Engineering, University of Bristol, Bristol, BS8 1TR, United Kingdom
[b] College of Engineering, Swansea University, Swansea SA2 8PP, United Kingdom
[c] Faculty of Engineering, University of Nottingham, Nottingham, NG7 2RD, United Kingdom
[d] School of Aeronautic Science and Engineering, Beihang University, Beijing, 100191, China
[e] College of Aerospace Engineering, Nanjing University of Aeronautics and Astronautics, Nanjing, 210016, China
[f] Ningbo Institute of Technology, Beihang University, Ningbo, 315800, China

ARTICLE INFO

Keywords:
Metamaterial
Morphing
Bend–twist coupling
Composite rotor blade
FE analysis

ABSTRACT

This work develops a morphing concept that utilises a metamaterial as the passive morphing device for helicopter blades. The metamaterials are created with bend–twist coupling, which enable the blade twist under prescribed bending loads. Finite element analysis (FEA) is performed to investigate the influence of the unit cell configurations on the coupling properties of the metamaterials. The numerical models are then validated experimentally through a set of bending tests conducted with additively manufactured prototypes. Finally, the validated model is used to design a graded metamaterial, where the cell aspect ratio gradually changes along the blade span, providing unique bend–twist coupling and allowing for tailored twist to be obtained. The results suggest the graded metamaterials are capable of introducing optimised nonlinear twists to the blade during different flight conditions including both hover and forward flight.

1. Introduction

Metamaterials allows the macroscopic material behaviours to be tailored by manipulating unit cell structures in the meso-, micro-, or even nano-scale, which enables unique material properties to be obtained at a very low density, such as negative Poisson's ratio, high resistance to damage or tunable dynamic properties [1–7]. Recent advances in morphing technologies allows adaptive blades to continuously change their shapes to achieve optimised performances throughout the entire flight envelope, calling for a new generation of metamaterials to be created to reduce design complexity and minimise the system weight.

Previous work has explored advanced functionalities of metamaterials such as negative compressibility, bi-stable, and shape adaptive structures [8–13]. Many metamaterials are capable of changing their shape by built in folding mechanisms; for example the self-folding origami lattices, which allow transformation between planar and large three-dimensional shapes, and are widely used in deployable space structures [14,15]. A similar type of deployable morphing was realised in many truss structures, such as the two-dimensional hexapod truss proposed by Onoda [16], where the morphing mechanisms were created by incorporating multiple sliding hinges to the structure design. However, a very high number of mechanisms and actuators will be required for such morphing process in order to achieve reasonable versatility of the structures. A variable geometry truss (VG-truss) concept was first exploited by Miura et al. [17], where a rigid static octahedral lattice was created using fixed-length beams, telescoping rods and hinge joints to enable geometric transformations of a robotic manipulator arm.

Advances in morphing blade concepts have led to a strong drive in developing radical smart structures, advanced materials, shape adaptive mechanisms, that allow blade shapes to be changed for different mission profiles to achieve improved aerodynamic performances [18–20]. Blade shapes are typically changed by twist, deflection of the trailing and leading edges, varying the sweep angles and span sizes [21–25]. Metamaterials such as chiral structures, have gathered significant interest in morphing blade concepts due to their inherent compliance and capability to withstand large strain such as chiral structures [26,27]. A passive camber morphing technique using metamaterials was investigated by Hyeonu et al. [28], where the airfoil sections were filled with various honeycombs such as the chiral, hexagonal and auxetic structures, allowing the leading and trailing edge to be passively deflected under aerodynamic forces. Similarly, Budarapu et al. [29] implemented auxetic metamaterials in a sized wing, where significant camber morphing was achieved, owing to the high deformability exhibited in the metamaterial. Sun et al. [30] proposed a morphing auxetic

* Corresponding author.
E-mail address: huaiyuan.gu@bristol.ac.uk (H. Gu).

https://doi.org/10.1016/j.compstruct.2022.116151
Received 19 March 2022; Received in revised form 5 June 2022; Accepted 13 August 2022
Available online 20 August 2022

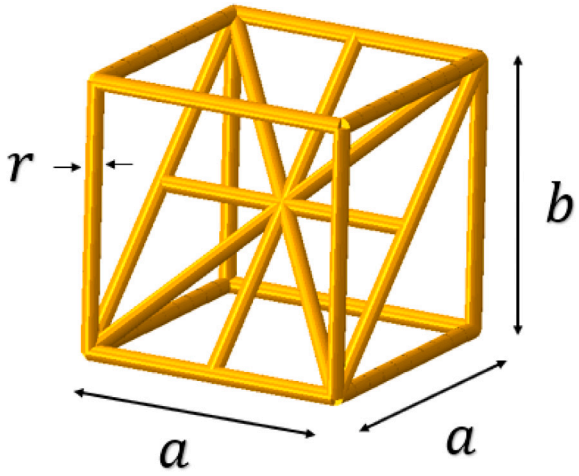

Fig. 1. The unit cell configuration of the metamaterial.

material which was designed to be placed between a hinge gap and can be employed as an actuator of a folding wingtip mechanism. The material consists of butterfly honeycombs with embedded inflatable pressure tubes in the unit cells. When the tube pressure is zero, the wingtip is able to free-flap around the hinge. While the tubes are pressurised, the material expands in all directions between the hinge gap due to its auxetic behaviour, leading to a strong recovery force to restore the wingtip to the original position. The potential of metamaterials in creating a large strain morphing skin was demonstrated by Jha et al. [31] using a Fish-Cell topology, where the measured failure strain was found to be beyond thirty.

Elastic coupling properties such as extension-twist and bend–twist are commonly employed in morphing blades as a passive or semi-passive mean to mitigate aerodynamic loads, improve aerodynamic performance and increase dynamic stabilities [32–34]. These properties are often achieved by tailoring the composite layup configurations e.g. symmetric and anti-symmetric layups [32,35], and the coupling coefficient can be effectively tailored by ply angles [36]. Raither et al. [37] developed a smart structure with tunable bend–twist properties by manipulating the shear rigidity of the webs using a layer of hard polyvinyl chloride (PVC), which in turn changes the position of the shear centre. Similar coupling properties may be obtained using three-dimensional metamaterials. For example the compression–torsion coupling can be realised by introducing twisted cells with inclined struts along the loading directions, such as tetra-chiral and Kirigami structures [38–40]. Furthermore, the coupling properties can be improved by carefully manipulating the cell geometric properties such as the number of cells in the transverse/longitudinal directions and angles and the number of the inclined struts. Highly effective tension–torsion coupling properties were experimentally measured from a 3D printed chiral honeycomb, where more than 10° of twist was achieved by applying an axial strain of 1% [41].

An inertial twist morphing concept has been proposed and explored extensively for rotor blade applications, which used a bend–twist coupled composite spar in the blade as a morphing device [42–44]. A movable mass at the blade tip generates an off-centred centrifugal forces to the blade, resulting in a lagwise bending moment, which in turn produces a coupled twist in the blade. It was shown that a reasonable level of blade twist can be actuated by using a small tip inertial mass. A bend–twist metamaterial proposed in a recent study was able to produce more efficient coupling properties compared to that achieved by composite beams created with a symmetric layup, leading to a reduction in the actuation energy required for the inertial twist concept [45]. However, few experimental studies exist to assess the accuracy of the numerical models. Furthermore, the blade twist demonstrated in the morphing concept only allows a linear twist along the blade span, whereas the optimum solutions of the blade twist are often found to be complex nonlinear forms [46–48].

Therefore, the aim of this paper is two-fold: (i) perform a comprehensive numerical analysis to determine the coupling properties achieved in bend–twist metamaterials and validate the numerical model using experimental methods. (ii) to improve the existing study that explore the potential of using graded metamaterials for morphing blade applications to obtain desired twist distributions. First, numerical analysis is conducted in Section 2 to investigate the behaviours of unit cell structures. Then a simple beam analysis is conducted in Section 3 to study the influence of the unit cell geometry on the coupling property of the metamaterial. Next, cantilever beam tests are reported in Section 4 that experimentally demonstrate the coupling property exhibited in the metamaterials, and the measured data are used to validate the numerical models. Finally, the validated models are utilised to design a graded metamaterial which allows the optimised blade twist to be achieved in different flight conditions.

2. Unit cell model

Fig. 1 shows a unit cell of the metamaterial which is comprised of a cubic cell and a triangulated bracing structure along its diagonal, leading to anisotropic modulus and coupling behaviour as revealed in [45]. The relative density, $\bar{\rho}$, of the metamaterial can be related to the dimensions of the unit cell as:

$$\bar{\rho} = \frac{3a + b + 2\sqrt{a^2 + b^2} + 2\sqrt{2a^2 + b^2}}{a^2 b}\pi r^2 \tag{1}$$

where r is the radius of the strut, a and b are the cell length and height. The aspect ratio (AR) of the cell is defined as the ratio between the cell length and width, a/b.

Finite element analysis (FEA) using ABAQUS 2017 was used to investigate the influence of the cell aspect ratio on their coupling properties. A set of unit cell models were created, where the width, a, and radius, r, were 8 mm and 0.5 mm respectively. The aspect ratio (AR), the ratio of b to a was varied between 1 to 5, as shown in Fig. 2. Note that the coupling between shear and direct strain can be negative if the cell orientation is changed in global beam coordinate system, see Section 5. Each strut was modelled by 10 Timoshenko beam elements(element type B31 in ABAQUS), where the elastic modulus and Poisson's ratio of the constituent material were assumed to be 70 GPa and 0.33. An axial loading, F_z, of 10 N was applied to each model while their bottom ends were fully fixed, as shown in Fig. 2. It can be seen that a shear strain was induced in each model subjected to the axial loading, F_z, due to the asymmetric features of the cell geometry. Fig. 3 shows the ratio between the induced shear strain, ϵ_{xz}, and axial strain, ϵ_{zz}, for the cells created with various aspect ratios (AR). It is clear that the higher strain ratio was obtained from the cells with the higher aspect ratios (AR), suggesting more effective coupling is achieved.

3. Beam models

3.1. Uniform metamaterial

A set of beam models were created by periodically stacking the unit cells described in Section 2, shown in Fig. 4, where x, y and z represent the local coordinate system of the unit cell and X, Y and Z represent the global coordinates of the beam. Five beam models were built with the same global dimensions by cells of various aspect ratio, AR, between 1 to 5, as shown in Fig. 5. Note that the unit cell is oriented in such way that the local y and z axes are parallel to the beam lateral and longitudinal directions respectively, so that each model is symmetric with respect to the $X-Z$ plane. Therefore a coupled torque will be induced when a lagwise bending moment, M_Z, is applied to the beam, due to the opposing shear strains, ϵ_{XZ}, induced in the tensile and

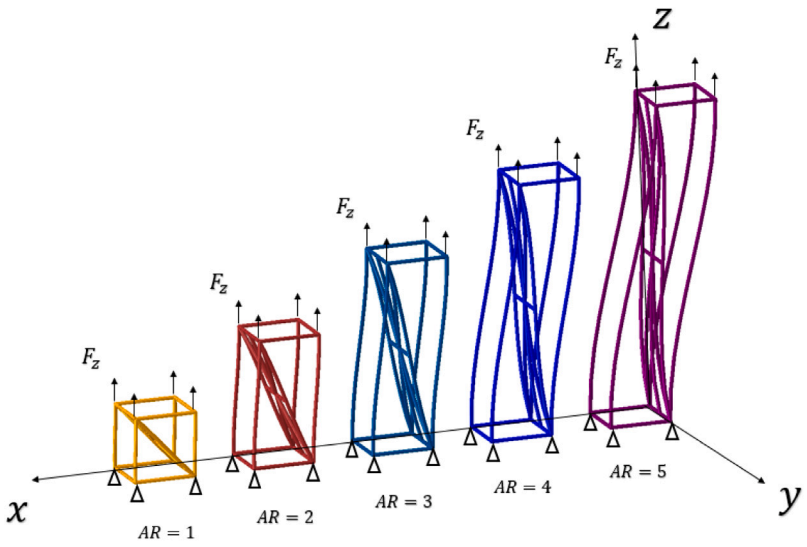

Fig. 2. Deformed unit cells created with various aspect ratios (AR).

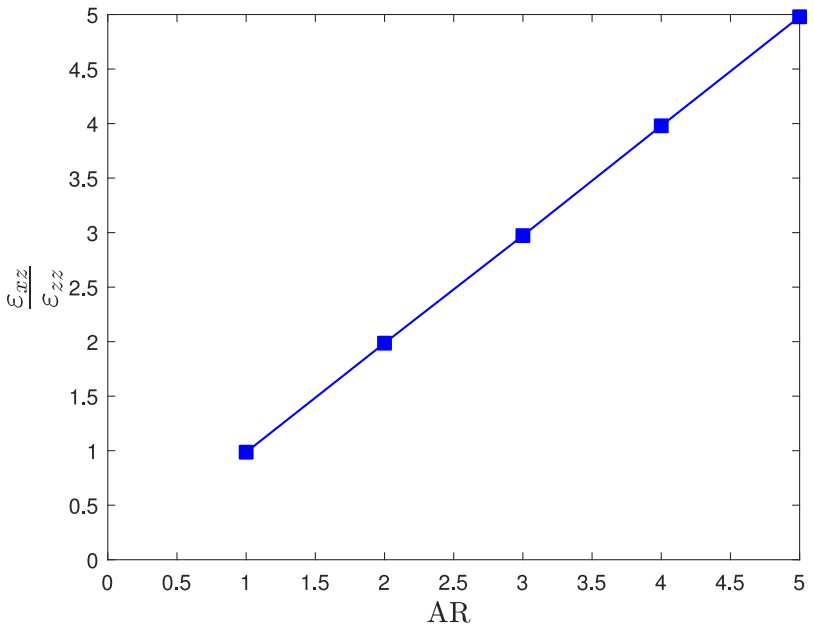

Fig. 3. The ratio between the coupled shear strain and applied axial strain for various unit cell aspect ratios (AR).

compressive side of the beam. According to the work of Hodge [49], the bend–twist property of an anisotropic beam can be characterised by the linear equations in a matrix form:

$$\begin{bmatrix} T_X \\ M_Z \end{bmatrix} = \begin{bmatrix} \overline{GJ} & -g \\ -g & \overline{EI} \end{bmatrix} \begin{bmatrix} \theta' \\ k_Z \end{bmatrix} \tag{2}$$

where the θ' and k_Z represent the rate of twist and lagwise bending curvature. T_X and M_Z are the applied torque and bending moment. $\overline{GJ}$, $\overline{EI}$ and g indicate the torsional, lagwise bending rigidity and coupling term of the beam. Therefore, the deflection and twist of the beam can be related to the applied moment and torque by a 2 by 2 stiffness matrix, where the individual elements in the matrix can be determined by performing a simple beam analysis on the numerical models. First a constant lagwise bending moment, M_Z, of 1 N m was applied to the tip of each model, while the root of the beams are fixed in all degree of freedoms. The corresponding distributions of the deflection and twist of the models are shown in Figs. 6 and 7, where the bending curvatures, k_Z, and rate of twist, θ' can be evaluated. Therefore Eq. (2) gives,

$$\overline{GJ}\ \theta'|_{M_Z=1} - g\ k|_{M_Z=1} = 0 \tag{3}$$

$$-g\ \theta'|_{M_Z=1} + \overline{EI}\ k|_{M_Z=1} = 1 \tag{4}$$

Similarly, when a unit torque, T_X, is applied to the tips of the beams, the rate of twist and corresponding coupled bending deflection can be obtained from the results, shown in Figs. 8 and 9, leading to expressions,

$$\overline{GJ}\ \theta'|_{T_X=1} - g\ k|_{T_X=1} = 1 \tag{5}$$

$$-g\ \theta'|_{T_X=1} + \overline{EI}\ k|_{T_X=1} = 0 \tag{6}$$

By solving Eqs. (3) to (6), the individual elements of the stiffness matrix can be determined, which are given in Table 1. It was found that the bending rigidity, $\overline{EI}$, is almost constant among the models, since $\overline{EI}$ is predominantly determined by the number and radius of the

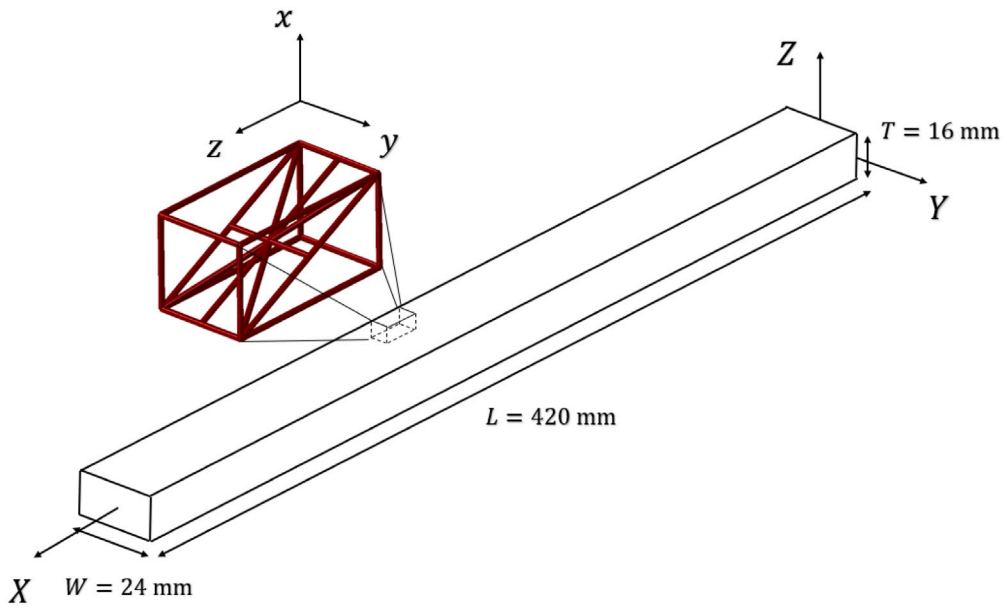

Fig. 4. Beam model created by the metamaterials.

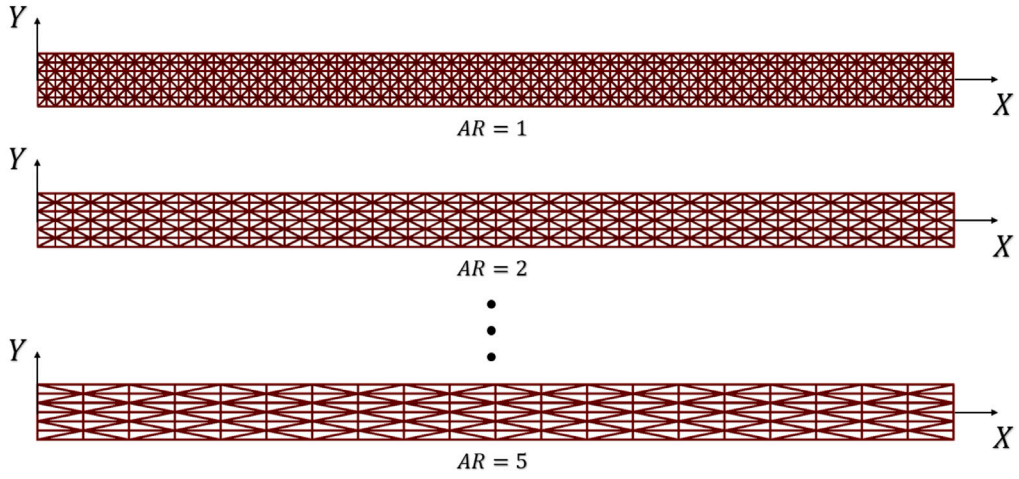

Fig. 5. Beam models composed of metamaterials with different aspect ratios.

struts parallel to the X-axis regardless of the change in the cell aspect ratio. It is shown that the coupling coefficient, α, defined as, $g/\sqrt{\overline{EI}\,\overline{GJ}}$, increases significantly with cell aspect ratio, AR, due to the inherent improvement in the extension-shear coupling property demonstrated in Fig. 3.

The stiffness matrix can be directly used to infer the bend–twist properties of the beams. The higher rate of twist is observed under a constant bending moment in the models created with the higher cell aspect ratio, shown in Figs. 6 and 7, whereas the bending deflection is almost identical. Conversely, for a beam subjected to a constant torque, the model with high aspect ratio cells gives rise to higher bending curvature as shown in Fig. 9. Furthermore, when AR is one, the sub cell is orientated at 45° to the axial direction of the beam, giving significantly enhanced torsional rigidity of the cells, leading to a higher torsional rigidity, $\overline{GJ}$, as shown in Table 1 and Fig. 8.

Table 1
Calculated values of the elements in the stiffness matrix.

AR	$\overline{EI}$ (N m^2)	$\overline{GJ}$ (N m^2)	g (N m^2)	α
1	58.0	1.06	0.47	0.06
2	57.6	0.82	0.75	0.11
3	56.0	0.86	1.17	0.17
4	56.7	0.88	1.59	0.23
5	58.9	0.87	2.0	0.28

3.2. Graded metamaterial

It has been shown that the cell aspect ratio is a key governing parameter to determine the stiffness matrix of the beams and their coupling behaviour. This section explores the bend–twist coupling of the metamaterials where the cell aspect ratio gradually changes along the beam span. Fig. 10 shows three beam models created with dimensions of 24 mm × 16 mm × 630 mm ($W \times T \times L$), and the cell aspect ratio is changed from 1 (at the beam root) to 5, 10 and 15 (at the beam tip), as shown in Fig. 11. The strut radius and material properties are identical to the model described in Section 3.1. A unit lagwise bending moment, M_Z, is applied to each model and the corresponding distribution of the twist and bending deflections are shown in Figs. 12 and 13. Significant changes in the twist distribution are seen compared to that observed in the uniform metamaterials shown in Fig. 8, where the coupled twists are quadratic where the rate of change increases along the beam span

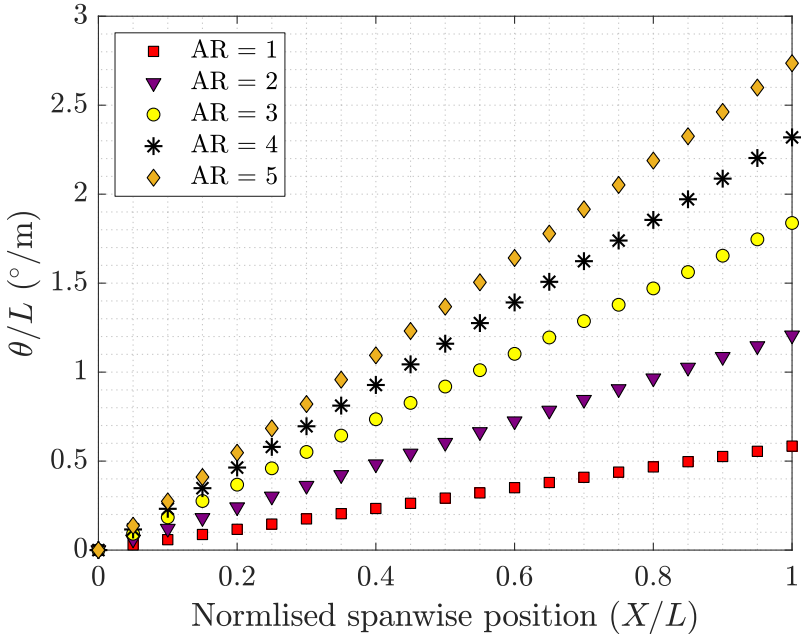

Fig. 6. Distribution of the twist in the beams subjected to a 1 N m lagwise bending moment at the tip.

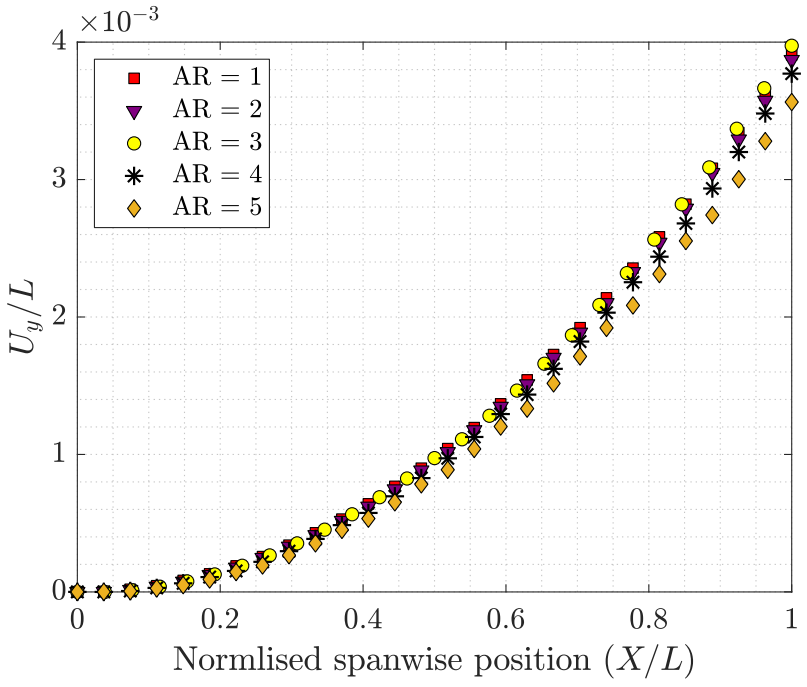

Fig. 7. Distribution of the deflection of the beams subjected to a 1 N m lagwise bending moment at the tip.

due to the increase in the cell aspect ratios. Furthermore, it is found that the Beam C created with a greater range of cell aspect ratio exhibits a higher level of nonlinearity in the coupled twist compared to that in Beams A and B, which enables the possibility of tailoring the twist distribution by manipulating the distribution of the cell aspect ratio. It is also shown that the change in cell aspect ratio will only cause a very small impact on the bending deflections, see Fig. 13.

4. Experimental validation

A set of samples were designed with same global dimensions but different cell aspect ratios, to investigate the validity of the numerical models used in the analysis. The strut radius, r, and cell length, l, are 0.5 mm and 8 mm respectively. Samples are fabricated by the PolyJet 3D printing process using a Stratasys J750 Digital Anatomy Printer with a minimum layer thickness of 20 μm. Layers of liquid photopolymer are applied by a jet onto the build tray during the printing process and instantly cured by UV light. The modulus and tensile strength of the material are 3000 MPa and 60 MPa. Solid sections are integrated into both ends of the samples for the ease of connection with the fixtures, as shown in Fig. 14.

Bending tests were performed with the cantilever beam configuration shown Fig. 15. The root of the sample was clamped by a pair of rigid metal plates, and a metal rod was installed at the tip, allowing various load cases to be applied to the beams, namely LC 0, LC 1 and LC 2. First, a 200 g mass was hung at the beam tip along

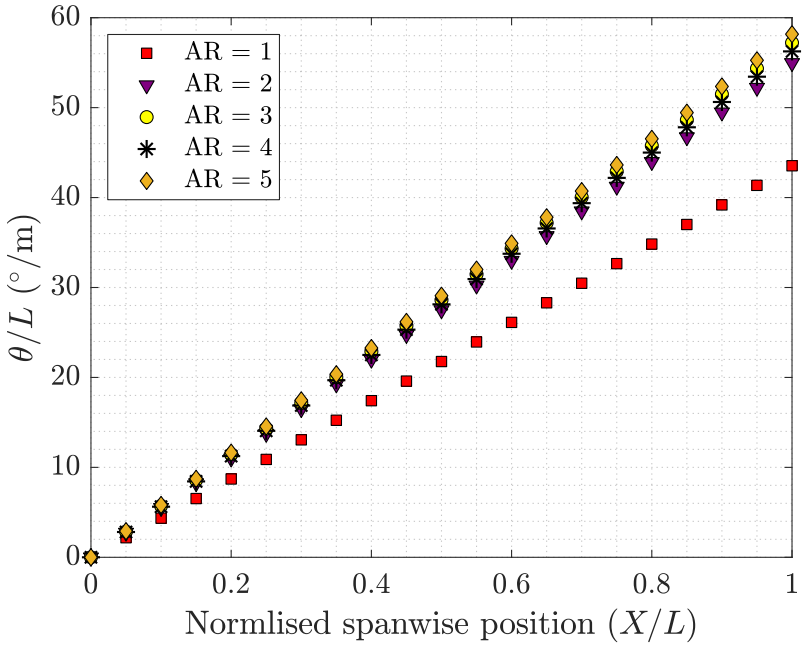

Fig. 8. Distribution of the twist of the beam subjected to a 1 N m torque at the tip.

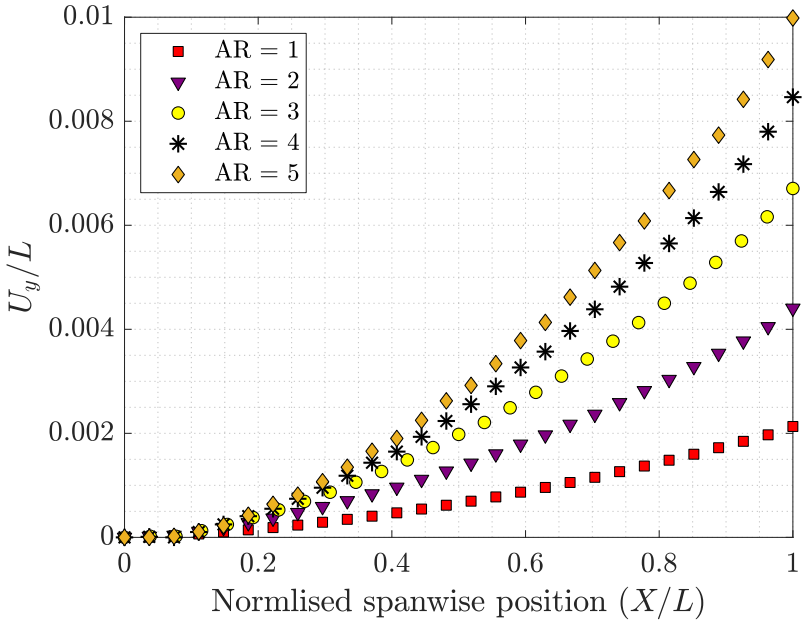

Fig. 9. Distribution of the deflection of the beam subjected to a 1 N m torque at the tip.

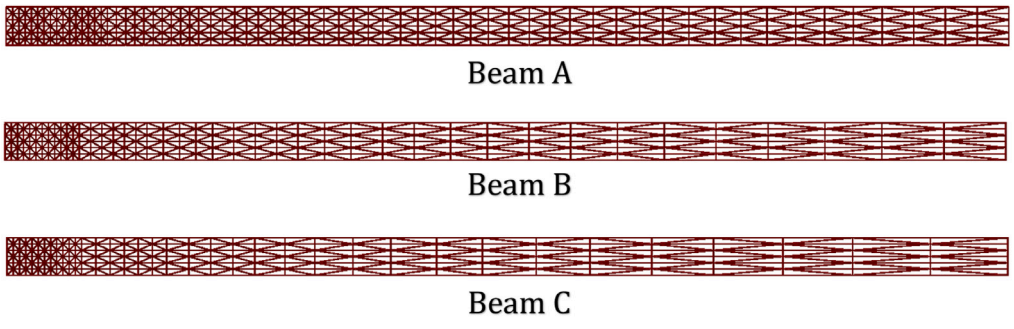

Fig. 10. Beams created by graded metamaterials with various range of cell aspect ratios.

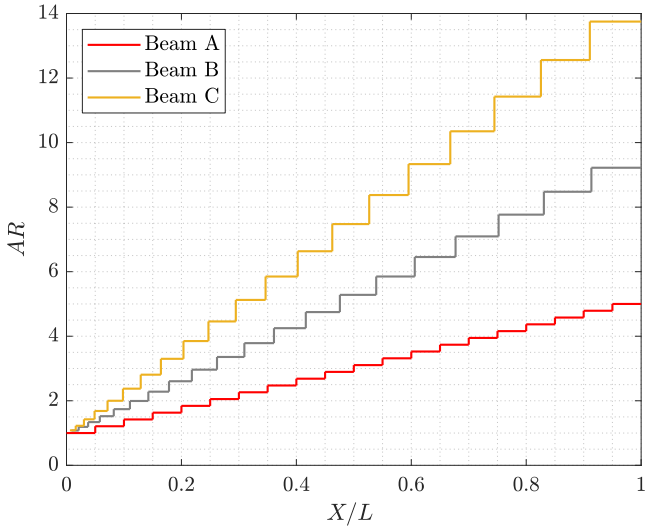

Fig. 11. Distribution of the cell aspect ratios in the graded metamaterials.

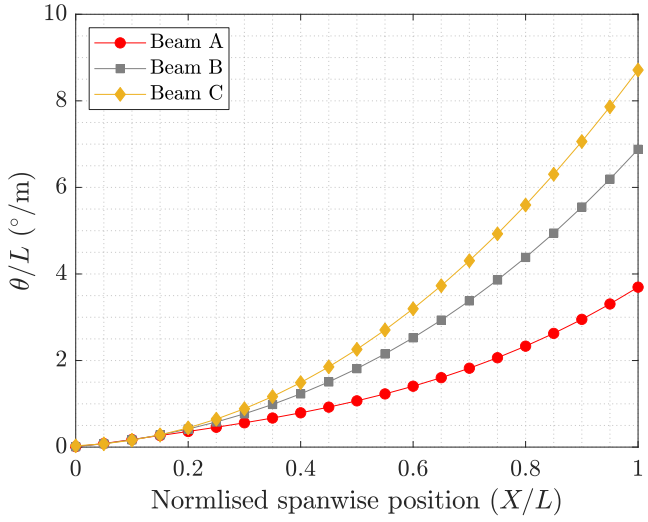

Fig. 12. Distribution of twist of models with graded cell aspect ratio subjected a 1 N m lagwise bending moment at the tip.

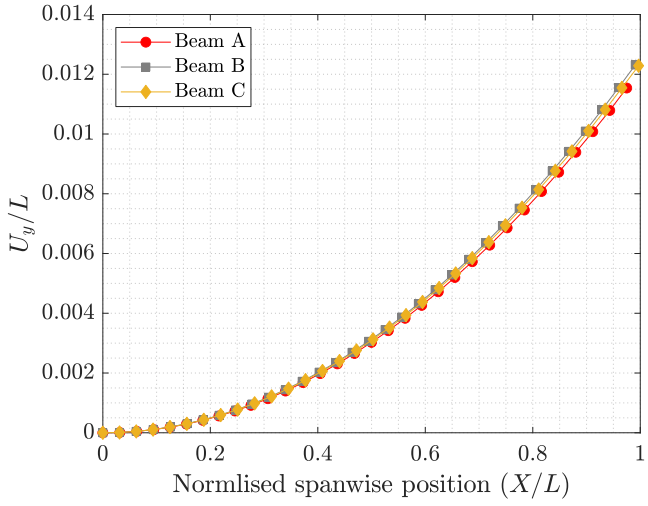

Fig. 13. Distribution of bending deflection of models with graded cell aspect ratio subjected to a 1 N m lagwise bending moment at the tip.

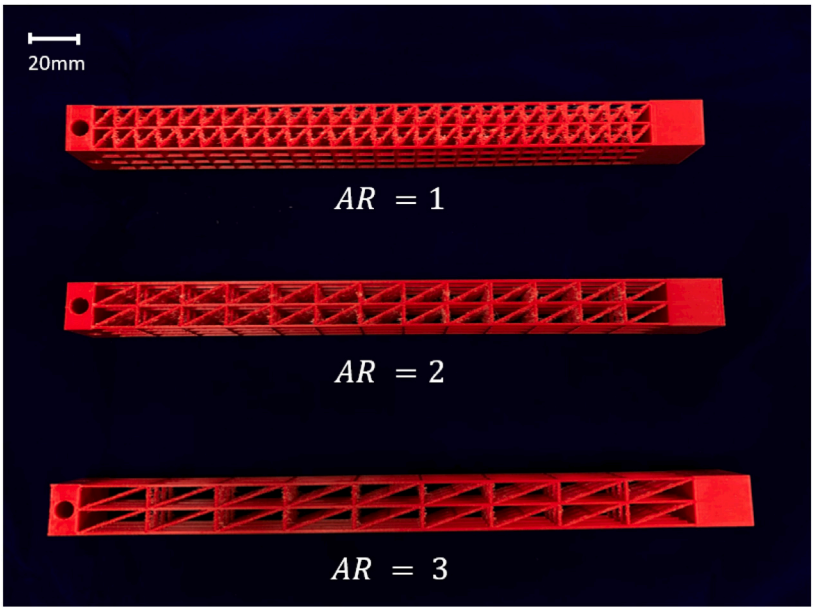

Fig. 14. Experimental beams with three different aspect ratios.

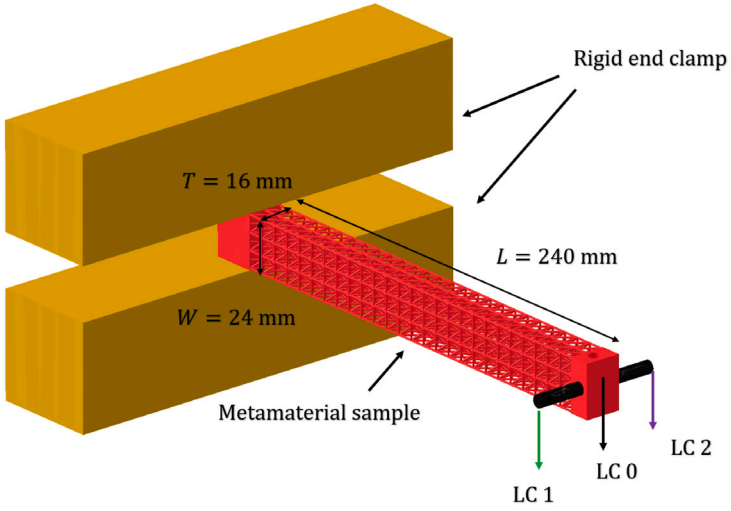

Fig. 15. Experiment setup for the bending test.

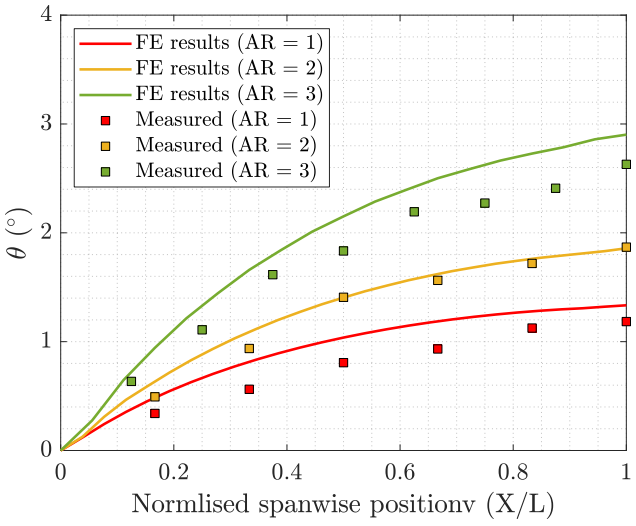

Fig. 16. Comparison of measured twist with FE results.

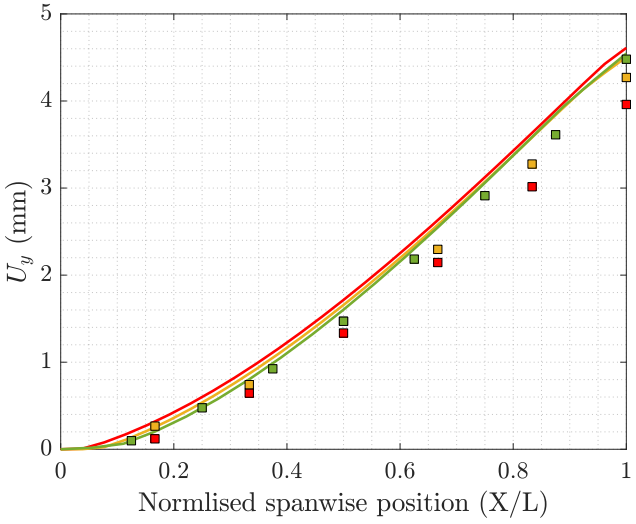

Fig. 17. Comparison of measured bending deflection with FE results.

the shear centre (LC 0), such that only bending moment and vertical shear force were introduced to the beams. Next, the mass was hung at position LC 1 and LC 2, in which the beam loading was mixed bending, vertical shear and torque. For each load case, the beam deflection and twist were measured using a pair of Omron laser sensors ZX2-LD 100, with a measurement range of 100 ± 35 mm and resolution of 5 μm, which captured the vertical and lateral displacements of the prescribed points on the beams. The sensors were set to zero after the metal rod was installed to ensure the displacements measured in the tests were induced by the applied tip mass.

Figs. 16 and 17 show the measured twists and vertical deflections of the beams subjected to a 200 g mass applied at the shear centre at the beam tip (LC0). The measured twist angle, θ, increases from the beam root to tip with a reduced rate of change, attributed to the linearly distributed bending moment along the beam span. It is clear that the greater twist angle, θ, was obtained from the samples with the higher cell aspect ratios, whereas the bending deflections were almost identical, which agrees well with the conclusion drawn in Section 3 and shown in Figs. 6 and 7. Fig. 18 compares the bending deflection and twist angle of the beams when the mass was applied at off-centred positions i.e. LC 1 and LC 2. Note that due to the presence of the bend–twist coupling, the magnitude of the twist angle, θ, was greater when the tip load was applied at LC 1, compared to that measured from LC 2, although the magnitude of the applied torques were identical. Similarly, the bending deflection seen in the load case LC 1 was higher than that measured from LC 2, as a result of the induced bending curvature caused by the applied torque. For LC 1, the induced bending moment was in the same direction as that applied at the tip, leading to an increased deflection. Conversely, a reduced deflection occurred when the torque was applied in the opposite direction (LC 2). Furthermore, the FE predicted results are compared to the measured data with good agreement, albeit with small differences. It was found that the FE predictions are higher than the measured data; a likely cause is that the FE model ignored the size of the strut joint, and underestimated the strut end effect.

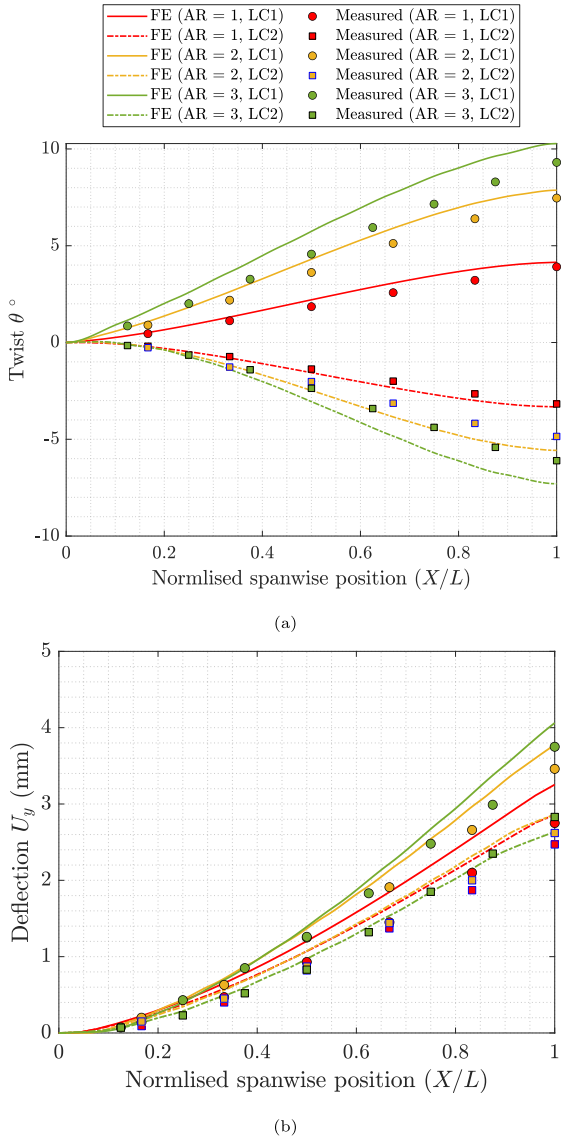

Fig. 18. Comparison between the distribution of (a) twist and (b)deflection of the samples subjected to off-centred loading.

5. Twist morphing for rotor blades

In this section, a morphing concept is proposed for helicopter blades which uses the bend–twist metamaterial as the core structure of a composite blade spar as shown in Fig. 19. The aim is to allow the optimum twists to be achieved in both hover and forward flight, where the optimised solutions are computed using a CFD-based optimisation approach performed by Leusink et al. [50] shown in Fig. 20. For the preliminary concept demonstration, a blade model was created with

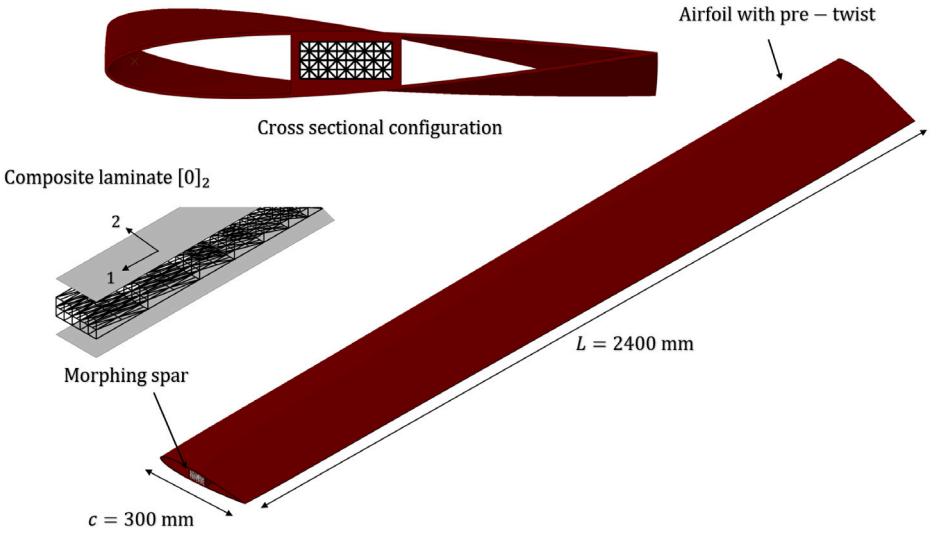

Fig. 19. Pre-twisted blade incorporating morphing spar made by composite skin and graded metamaterials.

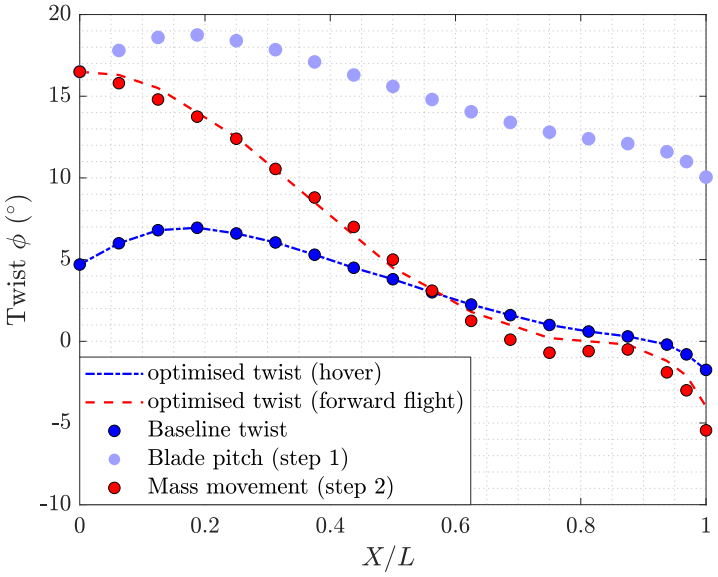

Fig. 20. Optimum twist distribution for helicopter blade during forward flight and hover.

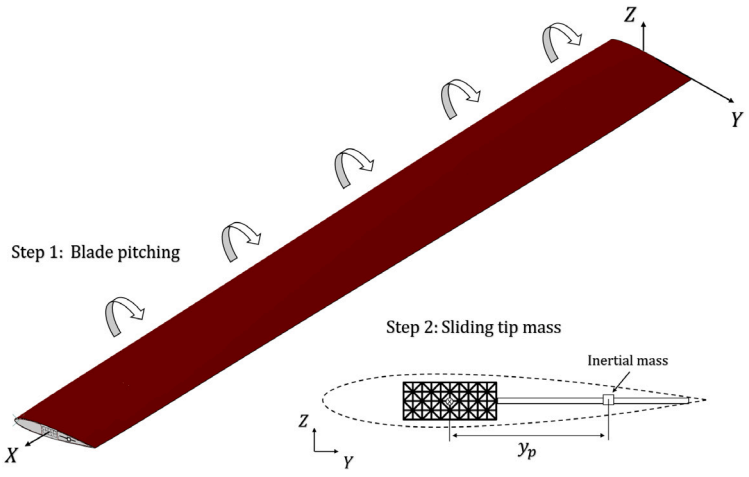

Fig. 21. Pre-twisted blade incorporating morphing spar made by composite skin and graded metamaterials.

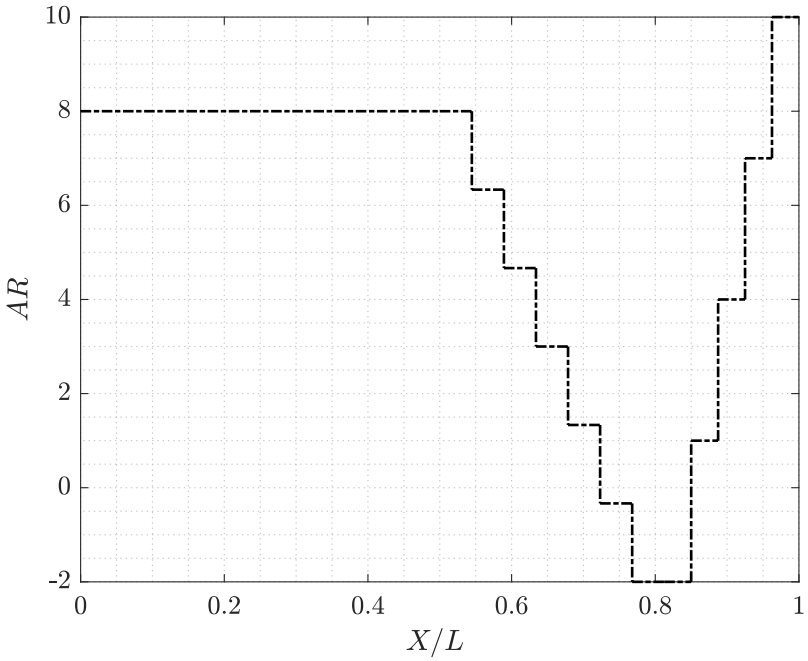

Fig. 22. Distribution of cell aspect ratio of the graded metamaterial.

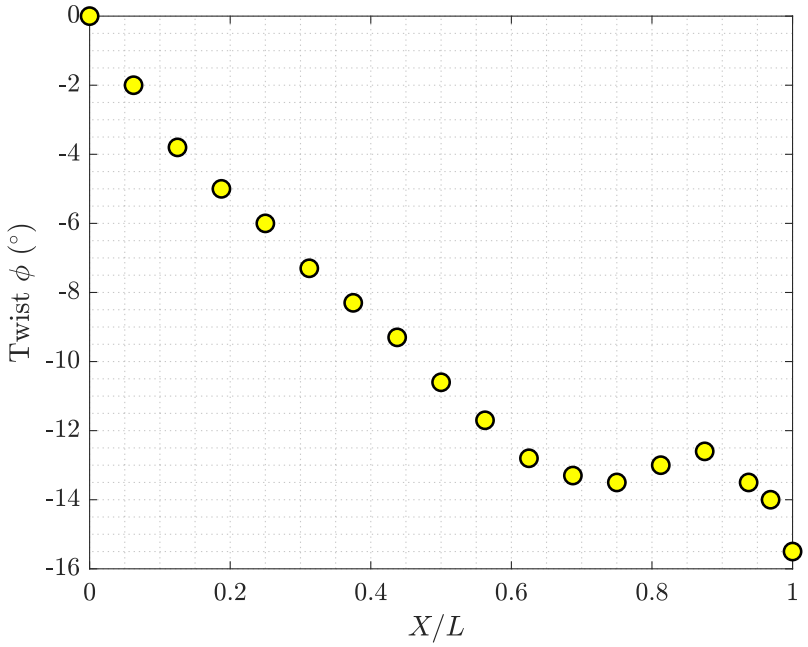

Fig. 23. Twist achieved in the graded metamaterial under prescribed rotational speed and tip mass position.

chord and span lengths of 300 mm and 2400 mm and the rotational speed was assumed to be 240 rpm. An initial twist was introduced to the blade model, based on the optimised twist distribution for hover (the blue dashed line shown in Fig. 20). A blade spar was designed as a sandwich structure, where the skins consisted of two layers of unidirectional 0° Hexcel 8522 IM7 carbon fibre laminate to withstand the axial loads caused by centrifugal forces, and the material properties of the laminate are shown in Table 2. Aluminium metamaterial was used in the core structure to drive the twist morphing in flight.

A two-step actuation process was designed for the blade including blade pitch control and position control of a tip inertial mass, as illustrated in Fig. 21, aiming to achieve the optimised blade twist during forward flight (the red dashed line shown in Fig. 20). Note that in this concept design, the impact of aerodynamic loads on the actuation mechanism and the corresponding system weight are not considered for the ease of analysis. The tip inertial mass was assumed to be 150 g, and was placed at the shear centre of the spar during hover, and moved to an off-centred position in forward flight, leading to a lagwise bending moment (caused by the centrifugal forces) and the coupled twist due to the bend–twist property of the morphing spar.

Table 2
Material properties used in the finite element(FE) model.

E_{11} (GPa)	E_{22} (GPa)	G_{12} (GPa)	υ_{12}	ρ (kg/m^3)
154	8.9	5.3	0.32	1400

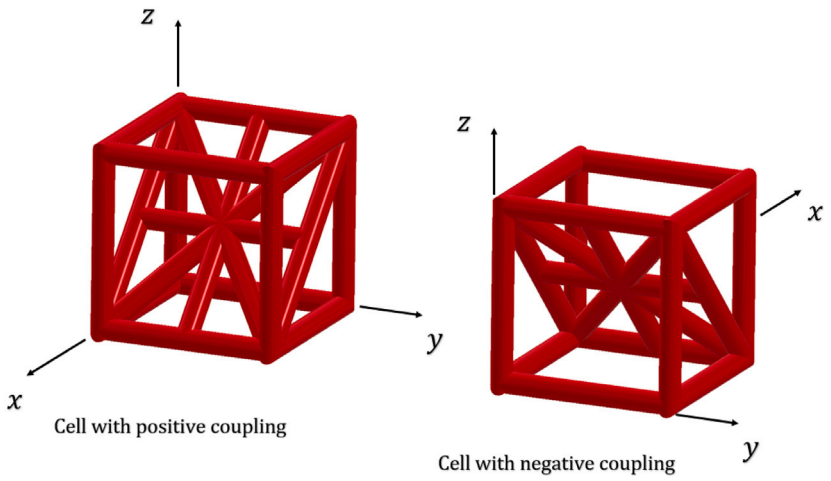

Fig. 24. Unit cells with positive and negative coupling.

In this particular case, the two-step actuation was performed by: (i) introducing a fixed pitch angle of 10° (ii) moving the tip inertial mass to an off-centred position with $y_p = 100$ mm.

To achieve the optimum shape for forward flight, the metamaterial was designed to generate a tailored negative (nose down) twist under the prescribed bending moment, as illustrated in Fig. 21. The cell aspect ratio was used as the design parameter to produce the targeted twist. Four design points were selected along the spar with normalised spanwise positions, X/L, of 0, 0.5, 0.8 and 1, whereas the aspect ratios of the cells between these points are linearly interpolated. An iterative process was undertaken to tune the bend–twist property based on the discrepancies between the blade twist and targeted twist i.e. a higher cell aspect ratio is applied in the subsequent analysis when a greater rate of twist is needed at the design points and vice versa. The evaluated distribution of cell aspect ratio and corresponding coupled twist are shown in Figs. 22 and 23. The cell aspect ratio was kept constant for $X/L < 0.5$ to produce a linear twist region, followed by a V-shaped distribution to enable a highly nonlinear twist to be obtained towards the tip of the spar. Note that the positive value of aspect ratio indicates the cell exhibited with positive coupling, where the local coordinate x-axis of the unit cell is in line with the X-axis of the beam global axis. While the negative sign in the aspect ratio suggests the x-axis of the cell is opposite to the X-axis of the beam, which leads to the negative coupling, (see Fig. 24). With this configuration, the optimised twist for forward flight was achieved, shown by the red dotted line in Fig. 20.

6. Concluding remarks

In this study, the coupling behaviour of a bend–twist metamaterial is investigated and the numerical models are validated using experimental data. A good agreement is achieved between the experimental results and numerical predictions, albeit with a small discrepancy which is likely caused by the strut end effects. The cell aspect ratio is the essential governing parameter to determine the coupling property: the higher the aspect ratio, the more efficient bend–twist coupling will be achieved. It is also found that a complex twist is able to be produced effectively by varying the distribution of cell aspect ratios along the beam. Furthermore, a concept design of a morphing rotor blade is proposed which utilises a graded metamaterial as a passive actuation device to induce tailored twists in flight. The preliminary demonstration shows that by carefully manipulating the cell aspect ratio, the optimised blade twist can be realised passively in both hover and forward flight conditions. Future study will address the detailed structural design to incorporate the metamaterials into the composite blades, allowing for an efficient twist morphing to be achieved while meeting design constraints.

CRediT authorship contribution statement

Huaiyuan Gu: Conceptualization, Methodology, Formal analysis, Investigation, Writing – original draft. **Javad Taghipour:** Investigation, Writing – review & editing. **Alexander D. Shaw:** Supervision, Project administration, Writing – review & editing. **Mohammadreza Amoozgar:** Writing – review & editing. **Jiaying Zhang:** Writing – review & editing. **Chen Wang:** Writing – review & editing. **Michael I. Friswell:** Supervision, Project administration, Writing – review & editing.

Declaration of competing interest

The authors declare that they have no known competing financial interests or personal relationships that could have appeared to influence the work reported in this paper.

Data availability

Data will be made available on request.

Acknowledgement

The authors acknowledge funding from the European Union's Horizon 2020 project 'Shape Adaptive Blades for Rotorcraft Efficiency (SABRE)', under grant agreement 723491.

References

[1] Lee W, Jeong Y, Yoo J, Huh H, Park S-J, Park SH, Yoon J. Effect of auxetic structures on crash behavior of cylindrical tube. Compos Struct 2019;208:836–46. http://dx.doi.org/10.1016/j.compstruct.2018.10.068.

[2] Gao Q, Liao W-H. Energy absorption of thin walled tube filled with gradient auxetic structures-theory and simulation. Int J Mech Sci 2021;201:106475. http://dx.doi.org/10.1016/j.ijmecsci.2021.106475.

[3] Zega V, Nastro A, Ferrari M, Ardito R, Ferrari V, Corigliano A. Design, fabrication and experimental validation of a MEMS periodic auxetic structure. Smart Mater Struct 2019;28(9):095011. http://dx.doi.org/10.1088/1361-665x/ab30be.

[4] Gu H, Pavier M, Shterenlikht A. Experimental study of modulus, strength and toughness of 2D triangular lattices. Int J Solids Struct 2018.

[5] Gu H, Li S, Pavier M, Attallah MM, Paraskevoulakos C, Shterenlikht A. Fracture of three-dimensional lattices manufactured by selective laser melting. Int J Solids Struct 2019;180–181:147–59.

[6] Gu H, Shterenlikht A, Pavier M. Brittle fracture of three-dimensional lattice structure. Eng Fract Mech 2019;219.

[7] Katia Bertoldi JC, van Hecke M. Flexible mechanical metamaterials. Nat Rev Mater 2017;2(66):17066. http://dx.doi.org/10.1088/1361-665x/ab30be.

[8] Nicolaou ZG, Motter AE. Mechanical metamaterials with negative compressibility transitions. Nat Rev Mater 2012;11(66):608–13, URL https://doi.org/10.1038/nmat3331.

[9] Yasuda H, Yang J. Reentrant origami-based metamaterials with negative Poisson's ratio and bistability. Phys Rev Lett 2015;114:185502. http://dx.doi.org/10.1103/PhysRevLett.114.185502, URL https://link.aps.org/doi/10.1103/PhysRevLett.114.185502.

[10] Cheung KC, Tachi T, Calisch S, Miura K. Origami interleaved tube cellular materials. Smart Mater Struct 2014;23(9):094012. http://dx.doi.org/10.1088/0964-1726/23/9/094012.

[11] Fenci GE, Currie NG. Deployable structures classification: A review. Int J Space Struct 2017;32(2):112–30. http://dx.doi.org/10.1177/0266351117711290.

[12] Isobe M, Okumura K. Initial rigid response and softening transition of highly stretchable kirigami sheet materials. Sci Rep 2016;6(66):24758, URL https://doi.org/10.1038/srep24758.

[13] Zheng Z, Xiangqi N, Helong W, Min S, Guanjun B, Huaping W, Shaofei J. Pneumatically actuated soft gripper with bistable structures. Soft Robot. 2022;9:57–71. http://dx.doi.org/10.1089/soro.2019.0195.

[14] van Manen T, Janbaz S, Ganjian M, Zadpoor AA. Kirigami-enabled self-folding origami. Mater Today 2020;32:59–67. http://dx.doi.org/10.1016/j.mattod.2019.08.001, URL https://www.sciencedirect.com/science/article/pii/S1369702119307394.

[15] Lv C, Krishnaraju D, Konjevod G, Yu H, Jiang H. Origami based mechanical metamaterials. Sci Rep 2014;4:5979, URL https://doi.org/10.1038/srep05979.

[16] Onoda J, Fu D-Y, Minesugi K. Two-dimensional deployable hexapod truss. J Spacecr Rockets 1996;33(3):416–21. http://dx.doi.org/10.2514/3.26776.

[17] Miura K, Furuya H, Suzuki K. Variable geometry truss and its application to deployable truss and space crane arm. Acta Astronaut 1985;12(7):599–607. http://dx.doi.org/10.1016/0094-5765(85)90131-6.

[18] Arrieta AF, Bilgen O, Friswell MI, Hagedorn P. Passive load alleviation bistable morphing concept. AIP Adv 2012;2(3):032118. http://dx.doi.org/10.1063/1.4739412.

[19] Barbarino S, Bilgen O, Ajaj RM, Friswell MI, Inman DJ. A review of morphing aircraft. J Intell Mater Syst Struct 2011;22(9):823–77.

[20] Fincham J, Friswell M. Aerodynamic optimisation of a camber morphing aerofoil. Aerosp Sci Technol 2015;27:245–55.

[21] III RDV, Kothera CS, Woods BK, Bubert EA, Wereley NM. One dimensional morphing structures for advanced aircraft. In: Agarwal RK, editor. Recent advances in aircraft technology. Rijeka: IntechOpen; 2012, http://dx.doi.org/10.5772/37333.

[22] Woods BK, Bilgen O, Friswell MI. Wind tunnel testing of the fish bone active camber morphing concept. J Intell Mater Syst Struct 2014;25(7):772–85. http://dx.doi.org/10.1177/1045389X14521700.

[23] Woods BKS, Dayyani I, Friswell MI. Fluid/structure-interaction analysis of the fish-bone-active-camber morphing concept. J Aircr 2015;52(1):307–19. http://dx.doi.org/10.2514/1.C032725.

[24] Johannes R, Srinivas V, van de Kamp Bram, Monner HP. Bench top test of a droop nose with compliant mechanism. Smart materials, adaptive structures and intelligent systems, Volume 2: Integrated System Design and Implementation; Structural Health Monitoring; Bioinspired Smart Materials and Systems; Energy Harvesting, 2015, http://dx.doi.org/10.1115/SMASIS2015-8853.

[25] Ajaj RM, Omar FK, Darabseh TT, Cooper J. Flutter of telescopic span morphing wings. Int J Struct Stab Dyn 2019;19(06):1950061. http://dx.doi.org/10.1142/S0219455419500615.

[26] Bettini P, Airoldi A, Sala G, Landro LD, Ruzzene M, Spadoni A. Composite chiral structures for morphing airfoils: Numerical analyses and development of a manufacturing process. Composites B 2010;41:133–47.

[27] Jamie M, Bruckner H, Jacques J, Chrystel R, Fabrizio S, Kevin P, Massimo R. The hexachiral prismatic wingbox concept. Phys. Status Solidi 2008;245:570–7.

[28] Hyeonu H, Jaehyung J, Doo-Man K, Chang-Soo J. Passive morphing airfoil with honeycombs. In: Proceedings of the ASME 2011 international mechanical engineering congress and exposition, Vol. 1, 2011, p. 263–71.

[29] Budarapu PR, B. SSY, Natarajan R. Design concepts of an aircraft wing: composite and morphing airfoil with auxetic structures. Front Struct Civ Eng Vol 2016;10:394–408. http://dx.doi.org/10.1007/s11709-016-0352-z.

[30] Sun J, Gao H, Scarpa F, Lira C, Liu Y, Leng J. Active inflatable auxetic honeycomb structural concept for morphing wingtips. Smart Mater Struct 2014;23(12):125023. http://dx.doi.org/10.1088/0964-1726/23/12/125023.

[31] Jha A, Dayyani I. Shape optimisation and buckling analysis of large strain zero Poisson's ratio fish-cells metamaterial for morphing structures. Compos Struct 2021;268:113995. http://dx.doi.org/10.1016/j.compstruct.2021.113995.

[32] Motley MR, Barber RB. Study on composite bend-twist coupled wind turbine blade for passive load mitigation. Compos Struct 2019;213:173–89.

[33] Stäblein AR, Hansen MH, Pirrung G. Fundamental aeroelastic properties of a bend–twist coupled blade section. J Fluids Struct 2017;68:72–89. http://dx.doi.org/10.1016/j.jfluidstructs.2016.10.010.

[34] Weisshaar TA. Aeroelastic tailoring of forward swept composite wings. J Aircr 1981;18(8):669–76. http://dx.doi.org/10.2514/3.57542.

[35] Meng H, Lien F-S, Glinka G, Geiger P. Study on fatigue life of bend-twist coupling wind turbine blade based on anisotropic beam model and stress-based fatigue analysis method. Compos Struct 2019;208:678–701. http://dx.doi.org/10.1016/j.compstruct.2018.10.032.

[36] Chandra R, Stemple AD, Chopra I. Thin-walled composite beams under bending, torsional, and extensional loads. J Aircr 1990;27:619–26.

[37] Raither W, Heymanns M, Bergamini A, Ermanni P. Morphing wing structure with controllable twist based on adaptive bending–twist coupling. Smart Mater Struct 2013;22:065017.

[38] Zhong R, Fu M, Chen X, Zheng B, Hu L. A novel three-dimensional mechanical metamaterial with compression-torsion properties. Compos Struct 2019;226.

[39] Wu W, Geng L, Niu Y, Qi D, Cui X, Fan D. Compression twist deformation of novel tetrachiral architected cylindrical tube inspired by towel gourd tendrils. Extreme Mech Lett 2018;20:104–11.

[40] Nayakanti N, Tawfic S, Hart AJ. Twist-coupled kirigami cells and mechanisms. Extreme Mech Lett 2018;21:17–24.

[41] Zheng B-B, Zhong R-C, Chen X, Fu M-H, Hu L-L. A novel metamaterial with tension-torsion coupling effect. Mater Des 2019;171:107700. http://dx.doi.org/10.1016/j.matdes.2019.107700.

[42] Gu H, Taghipour J, Rivero A, Amoozgar M, Shaw AD, Zhang J, Wang C, Friswell MI. Experimental validation of inertial twist concept for rotor blade application. Compos Struct 2022;288:115414. http://dx.doi.org/10.1016/j.compstruct.2022.115414.

[43] Gu H, Amoozgar M, Shaw AD, Zhang J, Wang C, Friswell MI. Experimental study of lag-twist coupling concept for rotor blade application. Compos Struct 2021;275:114417. http://dx.doi.org/10.1016/j.compstruct.2021.114417.

[44] Amoozgar M, Shaw A, Zhang J, Wang C, Friswell M. Lag-twist coupling sensitivity and design for a composite blade cross-section with D-spar. Aerosp Sci Technol 2019;91:539–47. http://dx.doi.org/10.1016/j.ast.2019.05.053.

[45] Gu H, Shaw AD, M. Amoozgarb JZ, Wang C, Friswell MI. Twist morphing of a composite rotor blade using a novel metamaterial. Compos Struct 2020;254:112855. http://dx.doi.org/10.1016/j.compstruct.2020.112855.

[46] Xie J, Xie Z, Zhou M, Qiu J. Multidisciplinary aerodynamic design of a rotor blade for an optimum rotor speed helicopter. Appl Sci 2017;7.

[47] Peters DA, Rossow MP, Korn A, Ko T. Design of helicopter rotor blades for optimum dynamic characteristics. Comput Math Appl 1986;12(1, Part A):85–109. http://dx.doi.org/10.1016/0898-1221(86)90089-1, URL https://www.sciencedirect.com/science/article/pii/0898122186900891.

[48] Imiela M. High-fidelity optimization framework for helicopter rotors. Aerosp Sci Technol 2012;23(1):2–16. http://dx.doi.org/10.1016/j.ast.2011.12.011, 35th ERF: Progress in Rotorcraft Research.

[49] Hodges DH. Nonlinear composite beam theory. American Institute of Aeronautics and Astronautics; 2006.

[50] Leusink D, Alfano D, Cinnella P, Robinet J-C. Aerodynamic rotor blade optimization at eurocopter - a new way of industrial rotor blade design. In: 51st AIAA aerospace sciences meeting including the new horizons forum and aerospace exposition. 2013, http://dx.doi.org/10.2514/6.2013-779.